ACS OMEGA

http://pubs.acs.org/journal/acsodf

Mini-Review

Carbon Dioxide Reduction Mediated by Iron Catalysts: Mechanism and Intermediates That Guide Selectivity

Ruggero Bonetto, Francesco Crisanti, and Andrea Sartorel*

Cite This: *ACS Omega* 2020, 5, 21309−21319

Read Online

ACCESS | Metrics & More | Article Recommendations

ABSTRACT: The reduction of carbon dioxide represents an ambitious target, with potential impact on several of the United Nations' sustainable development goals including climate action, renewable energy, sustainable cities, and communities. This process shares a common issue with other redox reactions involved in energy-related schemes (i.e., proton reduction to hydrogen and water oxidation to oxygen), that is, the need for a catalyst in order to proceed at sustainable rates. Moreover, the reduction of CO_2 faces an additional selectivity complication, since several products can be formed, including carbon monoxide, formic acid/formate, methanol, and methane. In this Mini-Review, we will discuss iron-based molecular catalysts that catalyze the reduction of CO_2, focusing in particular on the selectivity of the processes, which is rationalized and guided on the basis of the reaction mechanism. Inspired by the active sites of carbon monoxide dehydrogenases, several synthetic systems have been proposed for the reduction of CO_2; these are discussed in terms of key intermediates such as iron hydrides or Fe-CO_2 adducts, where the ligand coordination motif, together with the presence of co-additives such as Brønsted acids, nucleophiles, or CO_2 trapping moieties, can guide the selectivity of the reaction. A mechanistic comparison is traced with heterogeneous iron single-atom catalysts. Perspectives on the use of molecular catalysts in devices for sustainable reduction of CO_2 are finally given.

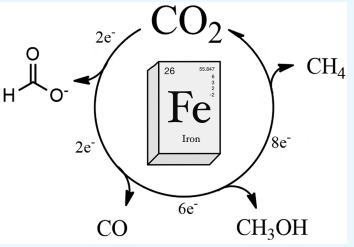

INTRODUCTION

The utilization of carbon dioxide as a ubiquitous raw material in the synthesis of commodity chemicals and for the production of solar fuels is an ambitious target; an efficient and large-scale exploitation of CO_2 could also help in reducing its impact as a greenhouse gas in the atmosphere. A few industrial processes have been realized where CO_2 is incorporated in organic chemicals for the production of linear and cyclic carbonates or salicylic acid;[1] conversely, processes leading to reduction of CO_2 are still not industrially developed. Issues associated with the reduction of CO_2 through electrochemical or photochemical processes are (i) the possibility of obtaining several products, such as carbon monoxide, formic acid or formate, methanol, and methane, which are discussed in this Mini-Review (eqs 1−5; potentials in aqueous medium are reported versus the normal hydrogen electrode, NHE; CO_2, CO, CH_4 are considered in the gaseous state, HCOOH, CH_3OH and H_2O in the liquid state, $HCOO^-$ in aqueous solution; see ref 2 for an extensive discussion of CO_2 reduction products); (ii) the requirement to use a catalyst to overcome the kinetic barriers associated with the multielectron/multiproton processes; and (iii) the competition of the hydrogen evolution reaction (eq 6) when proton donors are present in the reaction medium.

$$CO_2 + 2H^+ + 2e^- \rightleftharpoons CO + H_2O$$
$$E(CO_2/CO) = -0.11\ V - 0.0592 \times pH\ vs\ NHE \quad (1)$$

$$CO_2 + 2H^+ + 2e^- \rightleftharpoons HCOOH$$
$$E(CO_2/HCOOH) = -0.25\ V - 0.0592 \times pH\ vs\ NHE \quad (2)$$

$$CO_2 + H_2O + 2e^- \rightleftharpoons HCOO^- + OH^-$$
$$E(CO_2/HCOO^-) = -1.08\ V - 0.0592 \times pH\ vs\ NHE \quad (3)$$

$$CO_2 + 6H^+ + 6e^- \rightleftharpoons CH_3OH$$
$$E(CO_2/CH_3OH) = 0.02\ V - 0.0592 \times pH\ vs\ NHE \quad (4)$$

$$CO_2 + 8H^+ + 8e^- \rightleftharpoons CH_4 + 2H_2O$$
$$E(CO_2/CH_4) = 0.17\ V - 0.0592 \times pH\ vs\ NHE \quad (5)$$

$$2H^+ + 2e^- \rightleftharpoons H_2$$
$$E(H^+/H_2) = 0.00V - 0.0592 \times pH\ vs\ NHE \quad (6)$$

Received: June 12, 2020
Accepted: August 3, 2020
Published: August 20, 2020

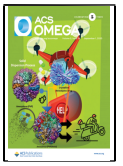

One of the most widely explored strategies to overcome the above issues is to exploit molecularly designed catalysts based on transition metal complexes, where comprehension of the reaction mechanism makes it possible to boost and drive the desired reactivity. Among the several systems investigated so far, a particular attention has been devoted to iron complexes, by virtue of the abundance of iron in the Earth's crust and its vast coordination chemistry and redox properties.

In this Mini-Review, we discuss mechanistic aspects of molecular iron catalysts toward the pathways of CO_2 reduction. Natural born Ni,Fe carbon monoxide dehydrogenases are first introduced. Synthetic iron complexes are then discussed: their peculiarities, despite constituting at first glance a variegated patchwork, can eventually be framed into rationally established categories, turning a vast literature scenario into a structured foundation. We focus in particular on the key competent intermediates, such as iron hydrides and iron-CO_2 adducts. In both cases, emphasis is given to the strategies to direct the selectivity of the process by means of co-additives such as Brønsted acids, nucleophiles, and CO_2 trapping moieties. Catalyst benchmarking will not be discussed, since it has been recently reviewed.[3]

NATURAL SYSTEMS FOR REVERSIBLE CO OXIDATION: Ni,Fe-CLUSTER IN CODHases

Through evolution, Nature has developed an important class of metalloenzymes to catalyze the reversible oxidation of CO to CO_2, using H_2O present in the environment as the source of oxygen. These biological catalysts belong to the class of carbon monoxide dehydrogenases (CODHases).

CODHases can be divided into two main categories, based on the nature of their active sites: Mo,Cu-based cofactors are used by aerobic bacteria, while a Ni,Fe-based active site is present in both archaea and anaerobic bacteria. In particular, the latter is part of a $[NiFe_4S_4]$-cluster (cluster C), where the nickel center, three iron atoms, and four sulfur atoms are assembled in a distorted cubane; the last Fe(II) ion (ferrous component II, FCII) is bound to a sulfur atom of the cubane and bears a hydroxide anion as an apical ligand, which is functional in the reactivity. Ni,Fe-based CODHases can be mono-, bi-, or even multifunctional. From a physiological perspective, while the former are able to catalyze only the CO oxidation, the latter are also capable of reducing CO_2, with the produced CO being involved in the acetyl-CoA synthesis taking place in a different subunit of the protein.[4−6]

From a mechanistic perspective, the states involved in the reversible oxidation of CO are named C_{red1}, C_{red2}-CO_2, and C_{red2} (Figure 1, clockwise cycle). Starting from the C_{red1} state, the binding of CO to the Ni^{2+} center occurs, together with the formation of a C−O bond between the carbon atom of CO and the oxygen of the OH group bound to FCII: this step results in the formation of the C_{red2}-CO_2 intermediate. As a matter of fact, in order to allow the formation of the new C−O bond, the coordination of CO to an equatorial position of Ni^{2+} is required; however, it is still unclear if the appropriate position is taken from the very beginning of the coordination process or it is reached by a fast "flipping" from an apical position. This uncertainty is due to the intrinsic difficulty in characterizing the state with CO coordinated to the cofactor, caused by its high reactivity.

The second step is the reaction of C_{red2}-CO_2 with H_2O to release CO_2 and $2H^+$, resulting in the formation of the C_{red2} state; in this state Ni is formally zerovalent, taking into account

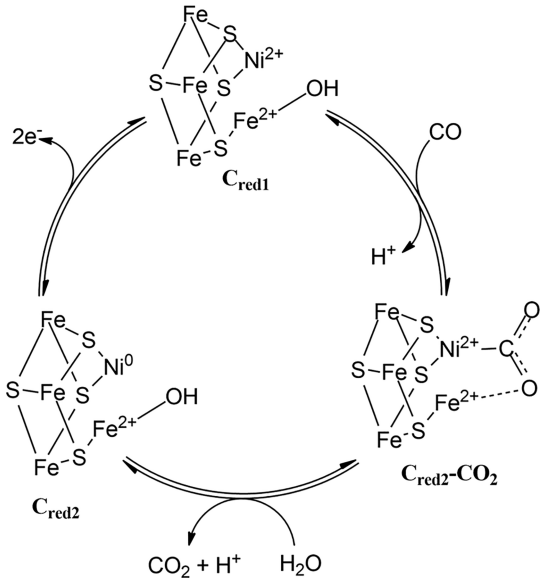

Figure 1. Mechanism of CO oxidation by Ni,Fe-CODHases involving the three states C_{red1}, C_{red2}, and C_{red2}-CO_2. It should be noted that the precise location of the two electrons contained in the C_{red2} state remains unclear. In the crystallographic structure of the C_{red}-CO_2 state, the CO_2 behaves as a μ^2,η^2 ligand, using the C atom to bind the Ni^{2+} metallic center and the O atom to coordinate the Fe^{2+}. This particular coordination geometry promotes CO production and hinders $HCOO^-$ formation in the counter-clockwise, reverse cycle of CO_2 reduction.

the oxidation process that occurred in the previous step. The last process that closes the cycle is the two-electron ($2e^-$) oxidation of C_{red2} to C_{red1}. A remarkable fact is that in this process the redox-active catalytic site is the $Ni^{2+/0}$ center, while the FCII acts as a Lewis acid and as a vessel for the hydroxo group.

Dobbek and co-workers[4] were able to obtain the crystallographic structure of the C_{red1} and C_{red2} states of cluster C from *Carboxydothermus hydrogenoformans*, with 1.40 Å resolution. Both C_{red1} and C_{red2} states show identical coordination geometry for the metals and similar $[NiFe_4S_4OH]$ structure: in these states, the Ni atom has a distorted T-shaped geometry with two sulfide ligands bound to the cluster and one thiol group from Cys^{526}; the Fe^{2+} ions of the cubane are tetracoordinated, showing sulfide ligands from the cluster or amino acid backbone ligands (mainly Cys). FCII is tetracoordinated and is bound to an amino group from His^{261}, a thiol group from Cys^{295}, a sulfide ligand from the cluster, and a hydroxo ligand.

In addition, Dobbek's group also characterized the C_{red2}-CO_2 state by adding $NaHCO_3$ to the C_{red2} state (moving therefore toward the opposite route with respect to the CO oxidation process, counter-clockwise direction in Figure 1).[4] The formal CO_2 coordination in C_{red2} takes place at the Ni and FCII metallic centers, with CO_2 behaving as a μ^2,η^2 ligand, where the C atom is bound to the distorted square planar Ni center with a short distance of 1.8 Å[5] and the O atom is coordinated to the FCII. The O−C−O angle decreases to 117° after coordination, while the C−O bond lengths increase to 1.30 and 1.32 Å; these features are consistent with the bound CO_2 being reduced by a $2e^-$ π-backbonding from the Ni center to the C-centered LUMO of CO_2. Therefore, in the C_{red2}-CO_2 state, Ni is formally recognized in the II oxidation state. The

https://dx.doi.org/10.1021/acsomega.0c02786
ACS Omega 2020, 5, 21309−21319

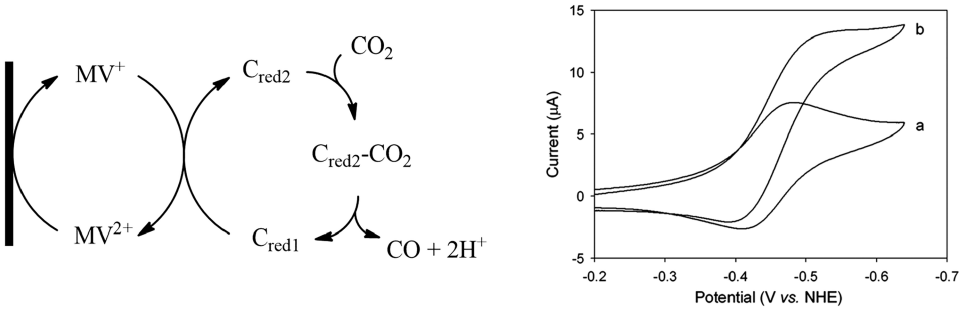

Figure 2. Left: Schematic representation of the electrochemical reduction of CO_2 to CO catalyzed by Ni,Fe-CODH. Right: Cyclic voltammograms obtained for the aqueous solutions containing MV^{2+} saturated with CO_2 with (b) and without (a) the enzyme. Adapted with permission from ref 6. Copyright 2003 American Chemical Society. C_{red1} is generated from an inactive state C_{ox} at applied potentials below −200 mV vs NHE, and is converted to C_{red2} via a two-electron reduction at a potential of −530 mV vs NHE, mainly ascribed to the reduction of the nickel center from II to 0.

partial negative charge present on the O atoms is stabilized via hydrogen-bonding interactions with the amino groups of His[93] and Lys[563].

The CODHases isolated from *C. hydrogenoformans* show a turnover frequency (TOF) of 31 000 s^{-1} and a k_{cat}/K_M of 1.7×10^9 M^{-1} s^{-1} for CO oxidation while working at 70 °C in buffered aqueous medium (pH = 8.0, 1 atm of CO) in the presence of dithioerythritol and of methyl viologen as a redox mediator. This result suggests that this system belongs to the class of the diffusion-limited perfect enzymes since its efficiency is only limited by the diffusion of CO in solution.[7] When the reverse process is considered, namely CO_2 reduction to CO, CODHases isolated from *Rhodospirillum rubrum* show a TOF of 45 s^{-1} and a k_{cat}/K_M of 2.5×10^6 M^{-1} s^{-1} while working at 25 °C and pH = 7.5, still in the presence of methyl viologen mediator and of dithionite as a chemical reductant.[8]

The ability of CODHases to catalyze the CO_2 reduction to CO in the presence of chemical reductants, together with the observation that the $E^{0\prime}$ of the $2e^-$ C_{red1}/C_{red2} couple is −530 mV vs NHE and close to the $E^{0\prime}$ of the CO_2/CO couple at neutral pH, led Shin and co-workers[6] to investigate Ni,Fe-CODH for the electrochemical reduction of CO_2 to CO. The study was conducted using a glassy carbon disk as working electrode, methyl viologen as redox mediator, CODHases from *Moorella thermoacetica* as electrocatalyst, and CO_2 as substrate in aqueous phosphate buffer at pH = 6.3 (Figure 2).

Comparing the cyclic voltammograms obtained in the presence and absence of CODHases, Shin's group demonstrated the catalytic effect of the enzyme, as indicated by the formation of a catalytic current at potentials below −0.4 V vs NHE, concomitant with the electrogeneration of C_{red2} from C_{red1} (Figure 2; C_{red1} can be generated from an inactive state of the enzyme C_{ox} at applied potentials below −200 mV vs NHE).[6] A deeper insight into this process was achieved by carrying out a controlled potential electrolysis (CPE) experiment at −0.57 V. According to the group's conclusions, the process is highly selective toward CO since no byproduct was detected with GC nor LC. CODHases are among the most efficient electrocatalysts for CO_2 reduction since the process occurs with overpotential as low as 0.09 V with respect to the $E^{0\prime}_{CO_2/CO}$ = −0.48 V at the same pH value (eq 1), and with a TOF of about 0.19 s^{-1}.

The elucidation of the structural features of the Ni,Fe site, together with the application of CODHases in artificial CO_2 electroreduction, prompted several research groups to design bioinspired synthetic catalysts for this transformation; some of them will be discussed in the next sections.

Fe-HYDRIDE INTERMEDIATES IN THE REDUCTION OF CO_2 TO FORMATE

Hydrides and Hydricity. The reactivity of a metal hydride (M-H) is associated with its hydricity, defined as the ability of the species to transfer a hydride H^-, and quantified as the free energy change ΔG_{H^-}(M-H) of the following reaction:[9]

$$\text{M-H} \rightleftharpoons \text{M}^+ + \text{H}^-; \quad \Delta G_{H^-}(\text{M-H}) \tag{7}$$

In order to transfer the hydride to CO_2 and transform CO_2 into formate (eq 8), the thermodynamic requirement sets $\Delta G_{EQ8} < 0$ (requirement 1); that is, ΔG_{H^-}(M-H) must be lower than the hydricity of formate, $\Delta G_{H^-}(HCOO^-)$, eq 9.

$$\text{M-H} + \text{CO}_2 \rightleftharpoons \text{M}^+ + \text{HCOO}^-; \quad \Delta G_{EQ8}$$
$$\Delta G_{EQ8} = \Delta G_{H^-}(\text{M-H}) - \Delta G_{H^-}(\text{HCOO}^-) \tag{8}$$

$$\text{HCOO}^- \rightleftharpoons \text{CO}_2 + \text{H}^-; \quad \Delta G_{H^-}(\text{HCOO}^-)$$
$$\Delta G_{H^-}(\text{HCOO}^-) = 44 \text{ kcal mol}^{-1} \text{ in CH}_3\text{CN};$$
$$24.1 \text{ kcal mol}^{-1} \text{ in water} \tag{9}$$

Kubiak and co-workers demonstrated that the hydricity of M-H can be predicted on the basis of the potential of the metal ion redox couples, and is solvent dependent.[9]

As a second condition, it should be noted that an exoergonic character of eq 8 does not itself guarantee the selective reactivity of the metal hydride M-H toward CO_2, since a competitive reaction with protons to produce hydrogen can occur (eq 10, where BH is a proton donor present in solution, required in electrocatalytic CO_2 reduction routines).[9]

$$\text{M-H} + \text{BH} \rightleftharpoons \text{M}^+ + \text{B}^- + \text{H}_2; \quad \Delta G_{EQ10} \tag{10}$$

Equation 10 can be considered as the sum of eq 7, eq 11, and eq 12:

$$\text{H}^- + \text{H}^+ \rightleftharpoons \text{H}_2; \quad \Delta G_{EQ11}$$
$$\Delta G_{EQ11} = -76 \text{ kcal mol}^{-1} \text{ in CH}_3\text{CN} \tag{11}$$

$$\text{BH} \rightleftharpoons \text{B}^- + \text{H}^+; \quad \Delta G_{EQ12}$$
$$\Delta G_{EQ12} = 2.303RT \times \text{p}K_a(\text{BH/B}^-) \tag{12}$$

https://dx.doi.org/10.1021/acsomega.0c02786
ACS Omega 2020, 5, 21309−21319

The ideal situation occurs when M-H is sufficiently reactive toward CO_2 ($\Delta G_{EQ8} < 0$, i.e., hydricity of M-H lower than the hydricity of $HCOO^-$, see requirement 1 above) but not reactive toward BH (i.e., $\Delta G_{EQ10} > 0$).[9] That is, $\Delta G_H^-(M\text{-}H) + \Delta G_{EQ11} + \Delta G_{EQ12} > 0$, which, inserting the definition ΔG_{EQ12}, results in $\Delta G_H^-(M\text{-}H) > -\Delta G_{EQ11} - 2.303RT \times pK_a(BH/B^-)$ (requirement 2).

Combining then requirement 1 and requirement 2: $-\Delta G_{EQ11} - 2.303RT \times pK_a(BH/B^-) < \Delta G_H^-(M\text{-}H) < \Delta G_H^-(HCOO^-)$.

In CH_3CN, at 298 K and expressing the free energies ΔG_{EQ11} and $\Delta G_H^-(HCOO^-)$ and RT in kcal mol^{-1}, this results in 76 $-1.364 \times pK_a(BH/B^-)$ kcal mol^{-1} < $\Delta G_H^-(M\text{-}H)$ < 44 kcal mol^{-1} (in CH_3CN).

Therefore, this relationship sets the basis for the choice of a proton donor BH with a suitable strength in order to direct the reactivity of M-H toward CO_2 reduction while avoiding H_2 evolution; the suitable $pK_a(BH/B^-)$ has thus a lower limit of ca. 23.46, while the appropriate range depends on the hydricity of M-H. In particular, the lower the hydricity $\Delta G_H^-(M\text{-}H)$, the higher the $pK_a(BH/B^-)$; i.e., for very reactive M-H, very weak BH acids are required.[9]

Iron Carbonyl Clusters. These considerations apply to the bioinspired, synthetic butterfly-like iron carbonyl clusters for CO_2 reduction to formate that have been reported by Berben and co-workers (Figure 3).[10,11] The forerunner and the most active in the series[11] is $[Fe_4N(CO)_{12})]^-$, hereafter abbreviated Fe_4N^-; a key feature of this species is the possibility of it being electrochemically converted to the one- and two-electron-reduced species, Fe_4N^{2-} (−1.23 V vs SCE) and Fe_4N^{3-} (−1.6 V vs SCE), in acetonitrile as aprotic solvent.[10] These intermediates are clearly distinguishable spectroscopically, showing different ν_{CO} stretching values in the range 1879−2018 cm^{-1};[10] a shift to lower wavenumbers upon reduction is consistent with the increase of electron density at the metal center, favoring the back-donation to π^* orbitals of the CO and thus the weakening of the CO bond.

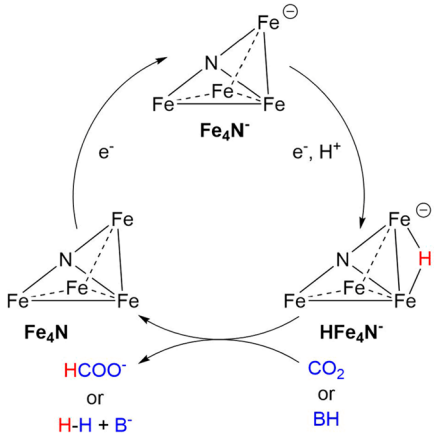

Figure 3. Electrogeneration of Fe hydride HFe_4N^- and its reactivity toward CO_2 or a Brønsted acid to generate formate or H_2, respectively. The 12 CO apical ligands of the Fe centers are omitted for clarity. Adapted with permission from ref 12. Copyright 2015 American Chemical Society.

The presence of protons in the medium allows the formation from Fe_4N^{2-} of a hydride species HFe_4N^- as a key intermediate. This species was also structurally characterized, and the hydride was located between two iron centers by analysis of the difference map.[12] In acetonitrile and in the presence of several Brønsted acids, HFe_4N^- electrocatalytically evolves H_2. Cyclic voltammetry analysis revealed the accumulation of HFe_4N^- when weak proton donors were employed, thus suggesting protonation of HFe_4N^- as the rate-determining step, consistent with the higher reaction rate observed in the presence of stronger acids (*p*-toluenesulfonic > chloroacetic > benzoic > butanoic). This evidence prompted Berben's group to exploit the slow reactivity of HFe_4N^- with "weak" butanoic acid, in order to direct it toward the reduction of CO_2.[10] Indeed, in the presence of CO_2, electrolysis gave formic acid as the main product; conversely, electrolysis in the presence of a stronger acid provided only H_2, even in the presence of CO_2, confirming that the H_2/HCOOH selectivity of the reaction could be directed by the strength of the proton donor.

The hydricity of HFe_4N^- was calculated from a thermochemical analysis to be +49 kcal mol^{-1} in acetonitrile and only 15.5 kcal mol^{-1} in water, thus impacting on the ΔG of eq 8: ΔG_{EQ8} changes from +5 kcal mol^{-1} in CH_3CN/water 95:5 (unfavored hydride transfer from HFe_4N^- to CO_2) to −8.6 kcal mol^{-1} in water (favored hydride transfer from HFe_4N^- to CO_2), thus predicting a more favorable driving force in aqueous medium. Indeed, in aqueous environment (pH range 5−13), the iron carbonyl cluster catalyzes CO_2 reduction to formate with a low overpotential (230−440 mV), a Faradaic yield (FY) up to 96%, and a TOF up to 3×10^{-2} s^{-1}.[12] Investigation of other iron carbonyl clusters led to less active and less selective processes, consistent with the thermochemical analysis predicting the hydricity of these species out of the optimal formate window.[11]

Besides the thermochemical analysis presented above, based on thermodynamic considerations, the reactivity of HFe_4N^- was investigated also on the basis of kinetic aspects, through an Eyring analysis aimed at determining the $\Delta G^{\ddagger}$ of the process, resulting in $\Delta G^{\ddagger}$ = 15.0 ± 0.1 and 12.3 ± 0.1 kcal mol^{-1} in CH_3CN/water 95:5 and in aqueous solution (pH 6.5), respectively.[13] The slightly different values for the two media suggest a common hydride transfer mechanism, with differ-

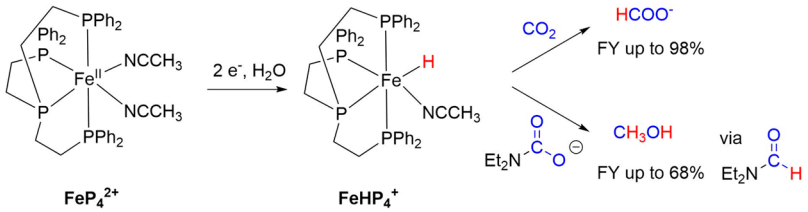

Figure 4. Formation of hydride intermediate $FeHP_4^+$ and the competitive pathways of reactivity for the direct reduction of CO_2, leading to formate, or the reduction of the carbamate of diethylamine, leading to formation of methanol via an *N,N*-diethylformamide intermediate.

https://dx.doi.org/10.1021/acsomega.0c02786
ACS Omega 2020, 5, 21309−21319

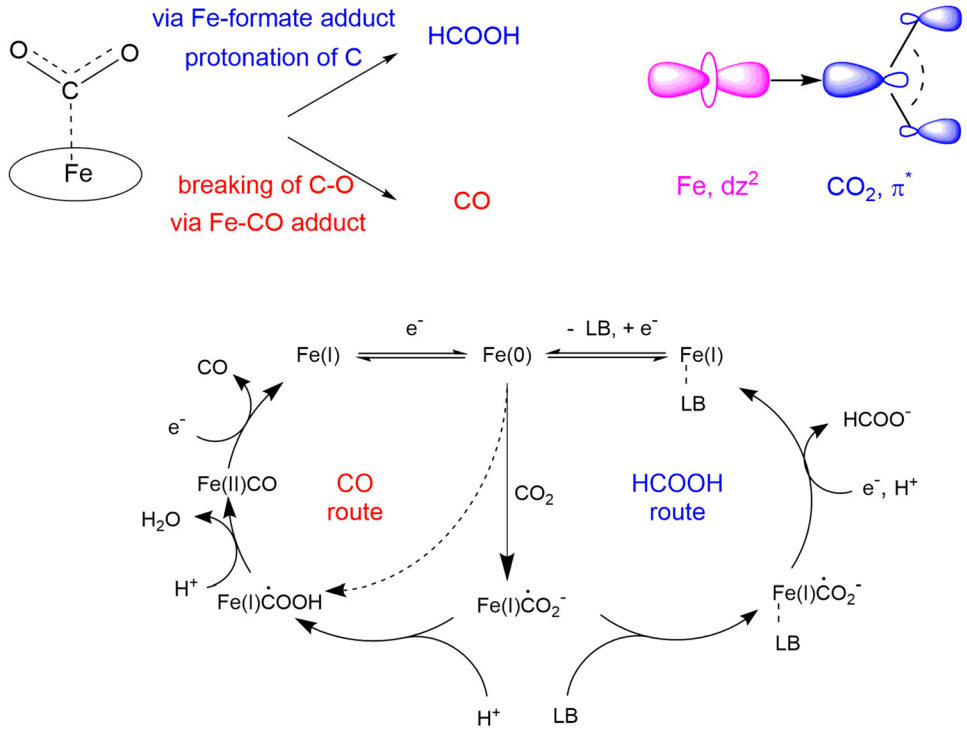

Figure 5. Top left: Representation of an η^1-C Fe-CO_2 adduct, and its evolution toward the production of formic acid (through protonation of carbon) or to carbon monoxide (upon cleavage of a C−O bond). Top right: General scheme representing electron donation from d_{z^2} of Fe to π^* of CO_2. Bottom: Catalytic cycle for iron porphyrins leading to CO[15−17] or to formic acid in the presence of Lewis bases (LB).[18] It is worth highlighting that the Fe(0) intermediate has been recently proposed to be an Fe(II) center with two reducing equivalents localized on the porphyrin ring.[19−21]

ences in transition-state structures, displaying a partial charge separation that can be likely solvated differently by the two media.

Mononuclear Fe Complex with Tetradentate Phosphine Ligand. A recent example of an iron species operating through a hydride intermediate for the conversion of CO_2 to formic acid was reported by Kang et al. (Figure 4).[14] This deals with a mononuclear Fe(II) complex with a tetradentate tris[2-(diphenylphosphino)ethyl]phosphine ligand, FeP_4^{2+}, that upon a $2e^-$ reduction to Fe(0) at $E_{1/2}$ = −1.13 V vs NHE in acetonitrile, in the presence of water, forms the Fe-hydride $FeHP_4^+$. This complex catalyzes the electrochemical reduction of CO_2 to formate with a Faradaic yield in the range 90−98%, depending on the amount of water (up to 10%) and on the applied potential (−1.0 to −1.6 V vs NHE), with H_2 being observed as the byproduct. An interesting effect that led to a drastic change in product distribution was observed upon addition of diethylamine: in this case methanol was obtained under electrolysis at −1.25 V vs NHE with a FY of up to 68%. The formation of methanol was attributed to the reduction of the carbamate formed from reaction of CO_2 with diethylamine, being competitive with the direct reduction of CO_2 to formic acid (Figure 4): indeed, the highest selectivity for methanol was obtained when the excess of residual CO_2 (i.e., the fraction that was not involved in carbamate formation) was removed from the solution. The authors identified *N,N*-diethylformamide as an intermediate product in methanol formation, since it initially accumulated during electrolysis, and was then consumed. Indeed, direct electrocatalytic reduction of *N,N*-diethylformamide led to methanol with a 90% Faradaic yield (Figure 4). Although several aspects of the mechanism still require further comprehension, the use of co-additives along with the catalyst to change the product selectivity and process efficiency is a most interesting topic that will likely be considered even more in future strategies for CO_2 reduction.

Fe-CO_2 INTERMEDIATES IN MONONUCLEAR IRON CATALYSTS

η^1-C Fe-CO_2 Adducts. In iron complexes for reduction of CO_2, key intermediates are mononuclear η^1-C Fe-CO_2 adducts, with CO_2 binding to iron in low oxidation states, typically I or 0. In most of the cases, the reactivity of such intermediates is directed either toward the formation of an Fe-CO adduct, upon breaking of a C−O bond assisted by protons, or toward the formation of a formate-type adduct, upon protonation of the carbon (Figure 5). These two routes ultimately lead to the production of CO and formic acid, respectively. The selectivity of the process depends on the nature of the η^1-C Fe-CO_2 intermediates, where the Fe−carbon bond is characterized by a significant electron density donation from the metal center to the π^* orbitals of CO_2. It is recognized that a high electron density of the iron center leads to a higher retrodonation, with the effect of increasing the electron density and the basicity of the carbon center. This ultimately favors protonation of carbon and the route toward formic acid.

CO_2 Reduction by Iron Porphyrins to CO. Among mononuclear iron complexes, Fe porphyrins have been the most investigated class of catalysts for CO_2 reduction.[15−17] Such catalysts display high reactivity and selectivity toward CO, and represent the forerunner category from both the application and the mechanistic knowledge standpoints. The catalytic mechanism proceeds through reaction between CO_2

https://dx.doi.org/10.1021/acsomega.0c02786
ACS Omega 2020, 5, 21309−21319

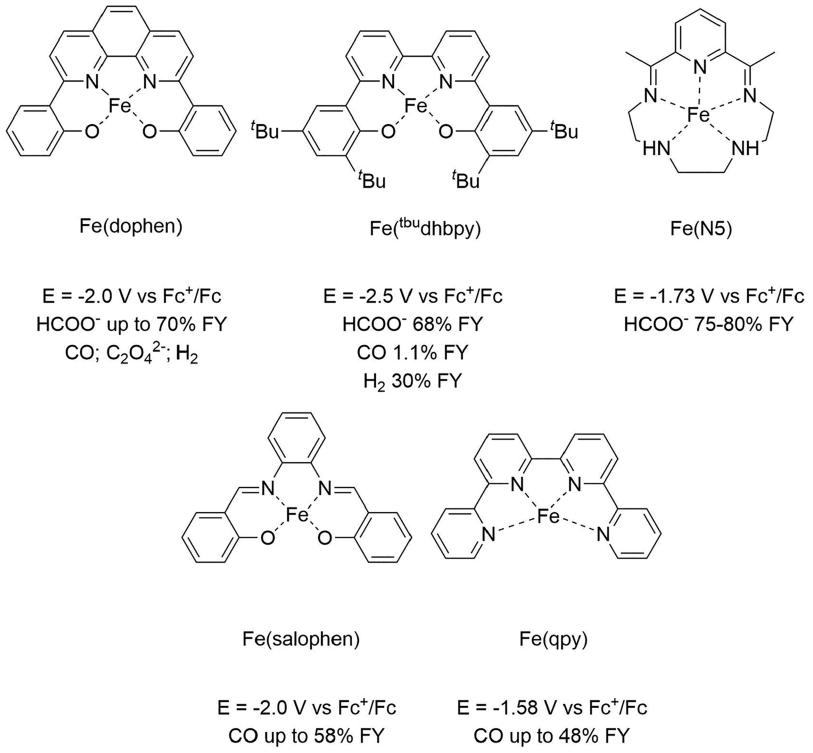

Figure 6. Structural representation of Fe(dophen), Fe(^{tbu}dhbpy), Fe(N5), Fe(salophen), and Fe(qpy), and summary of selectivity in the electrochemical reduction of CO_2. Apical ligands are omitted for clarity. These catalysts are all active through an Fe(I) intermediate.

and the Fe(0) active form of the catalyst: the resulting adduct is typically represented as an $Fe(I)CO_2^{\bullet-}$ (Figure 5),[15−17] although the actual electron distribution is more properly depicted through the contribution of resonance formulas $Fe(II)CO_2^{2-}$ and $Fe(0)CO_2$.

Spectroscopic investigation of iron tetraphenylporphyrin (Fe-TPP) intermediates with CO_2 was carried out by Mondal et al. under cryogenic conditions, upon a chemical reduction of the Fe-TPP catalyst.[22] The authors isolated the $Fe(I)CO_2^{\bullet-}$ adduct, which is then readily protonated by weakly protic solvents to form a long-lived Fe(I)ĊOOH species (Figure 5, see the CO route). In agreement with previous observations, this protonation step is believed not to be rate-determining: indeed, upon increasing the proton donor strength (i.e., using phenol), the $Fe(I)CO_2^{\bullet-}$ complex was not detectable, since the Fe(0) intermediate is directly converted to the FeĊOOH intermediate (dashed arrow in Figure 5).

Both $Fe(I)CO_2^{\bullet-}$ and Fe(I)ĊOOH intermediates were identified by resonance Raman spectroscopy. The $Fe(I)CO_2^{\bullet-}$ adduct displayed a signal in the low-frequency region at 590 cm^{-1}, attributed to stretching of the Fe−C bond, that shifts to 521 cm^{-1} in Fe(I)ĊOOH upon protonation. The Fe(I)ĊOOH intermediate also displayed a FT-IR signal at 1573 cm^{-1}, attributed to the C−O stretching of the COOH moiety.[22] This represents a rare finding in terms of intermediate detection in the field of iron-catalyzed CO_2 reduction, since most commonly identified species are indeed inactive iron carbonyl complexes (*vide infra*).

The second protonation event involves Fe(I)ĊOOH and leads to the cleavage of the C−O bond, with loss of one water molecule and formation of an Fe(II)CO. At this stage, a further one-electron reduction of Fe(II) to Fe(I) is needed in order to release CO from the iron coordination sphere; this is justified on the basis of the lower affinity to CO of Fe(I) with respect to Fe(II).[23−25] The Fe(II)CO adduct formation is suggested by the appearance of new anodic peaks in the CV of CO_2-saturated solutions of Fe-porphyrin catalysts.[15−17] This complex is generated upon re-oxidation at −1.6 V vs SCE of a CO_2-saturated solution of Fe-TPP in dimethylformamide (DMF) after electrolysis at a potential value at which CO_2 is catalytically reduced (−1.8 V vs SCE).[23] Furthermore, spectroelectrochemistry (SEC) in the UV−visible range has provided evidence of such a Fe(II)CO intermediate, displaying a Soret band at 420 nm.[26] Incidentally, this last stage of the catalytic cycle is reminiscent of the well-known high affinity of heme complexes for CO. It is therefore possible to draw a parallel, based on the properties of the iron(II) porphyrin carbonyl complex, between these catalytic systems and the biochemical routes of blood poisoning involving carbon monoxide coordination to oxygen-binding heme proteins.[27]

As a final remark, it is worth highlighting the crucial, two-fold role of Brønsted acids in the Fe-porphyrin cycle: they are proton donors, i.e., co-substrates in the reaction, and co-catalysts. Indeed, as well as Lewis acids, they participate in a push−pull scheme in which the iron complex injects electron density into CO_2 by back-donation, while the co-catalyst interacts with the substrate through its oxygen atoms by electrostatics and/or hydrogen bonding. This provides a stabilizing effect on the Fe-CO_2 adduct and weakens the C−O bond after the first, protonation step. Outstanding catalytic performance could be achieved by installing such co-catalytic units into iron's second coordination sphere. This strategy allows simultaneous activation of the CO_2 substrate, stabilization of key intermediates, and selectivity enhancement toward CO.[28−31]

CO_2 Reduction by Iron Porphyrins to Formate. Recently, Margarit et al.[18] achieved switching the selectivity of Fe-TPP from CO toward formate (up to 68% FY with

https://dx.doi.org/10.1021/acsomega.0c02786
ACS Omega 2020, 5, 21309−21319

phenol proton donor) by employing tertiary amine co-additives, acting as monodentate ligands to iron in the trans position with respect to CO_2 (Figure 5).[18] This peculiarity is justified by an enhanced Fe→CO_2 electron density transfer upon coordination of the amine, inducing an increase of the basicity of the carbon atom of coordinated CO_2, and thus favoring the formic acid route (Figure 5). The back-bonding ability of the iron center in heme systems is indeed promoted by basic trans ancillary ligands; in this case a reactivity trend is observed in the series quinuclidine > trimethylamine > diisopropylethylamine.[18]

The reported CO-to-HCOOH change of selectivity is remarkable, since in this case no iron hydride intermediate is involved toward the formation of formate, and thus the possible competitive evolution of hydrogen is negligible.[18] It is worth highlighting that tertiary amines are often employed in photocatalytic cycles for the reduction of CO_2;[32,33] the evaluation of their effect on the selectivity of the process in these systems should be thus considered.

CO_2 Reduction by Iron Porphyrins to Methane. As discussed above, the release of CO from iron porphyrins involves a one-electron reduction of the Fe(II)CO adduct, regenerating the Fe(I) resting state (Figure 5). Under electrocatalytic conditions, the CO release is fast since it occurs in the reaction−diffusion layer at the electrode, whose potential during electrolysis favors the Fe(0) and Fe(I) oxidation states. The fast release of CO by iron porphyrins has been known to drive the reduction of CO_2 to this $2e^-/2H^+$ CO route for this class of catalysts.[15−17] Conversely, when CO_2 reduction is conducted with photocatalytic systems, the Fe(II)CO adduct may accumulate to a non-negligible extent, since its further reduction requires a bimolecular reaction with the reduced photosensitizer. Therefore, subsequent reactions that involve participation of CO in the coordination sphere of the iron catalyst may occur.

Indeed, two recent literature examples report that, under optimized photocatalytic conditions, the complete $8e^-/8H^+$ reduction of CO_2 to CH_4 can be achieved with a remarkable selectivity of 14−15%,[34,35] employing an iron catalyst bearing a quaternary ammonium-functionalized porphyrin ligand. In the first report, $Ir(ppy)_3$ was used as photosensitizer,[34] while in a more recent work this role was played by a phenoxazine chromophore.[35] These peculiar and novel examples highlight how tuning of the system allows new catalytic routes to be exploited by overcoming extrinsic mechanistic barriers.

Non-heme Iron Mononuclear Complexes. Non-heme mononuclear iron complexes have been developed as another class of catalysts for CO_2 reduction, with mechanistic details and principles being common to both categories (Figure 6).[36−40] However, differently from the previously discussed iron porphyrins, these systems share the common feature of operating through a formal Fe(I) intermediate.

Three of these catalysts deal with iron complexes with N_2O_2 tetradentate ligands: 2,9-bis(2-hydroxyphenyl)-1,10-phenanthroline (H_2dophen), 6,6′-di(3,5-di-*tert*-butyl-2-hydroxybenzene)-2,2′-bipyridine (^{tbu}dhbpy), and *N*,*N*′-*o*-phenylenebis(salicylimine) (H_2salophen); the 2,2′:6′,2″:6″,2‴-quaterpyridine (qpy) and 2,13-dimethyl-3,6,9,12,18-pentaazabicyclo[12.3.1]octadeca-1(18),2,12,14,16-pentaene (N5) provide instead nitrogen-based planar tetradentate and pentadentate motifs, respectively.

Fe(dophen) catalyzes the reduction of CO_2 through an Fe(I) intermediate, generated in DMF or dimethyl sulfoxide at $E = -2.0$ V vs Fc^+/Fc, in the presence of proton donors;[36] the nature of these latter has an impact on the selectivity of the process, where the main product is formate (FY up to 70%), while CO, $C_2O_4^{2-}$, and H_2 were also observed. This observation was reasoned on the basis of two competitive pathways, one involving a postulated Fe-hydride intermediate, and the second one involving an η^1-C Fe-CO_2 adduct. The former is responsible for formate and H_2 evolution (see also previous paragraph; in this case SEC-IR suggested the involvement of an iron-formato species, Fe-OC(O)H, 1328 cm^{-1}); the Fe-CO_2 adduct is involved in CO and oxalate formation. SEC-IR revealed also the accumulation of an iron-carbonyl species (Fe-CO, 1934 and 1881 cm^{-1}) before evolution of CO (2140 cm^{-1}).

A similar scenario involving two competitive pathways was hypothesized for Fe(^{tbu}dhbpy),[37] which shows a higher selectivity for formate (up to 68% FY at −2.5 V vs Fc^+/Fc with phenol proton donor, with ca. 1% FY for CO). Also in this case the active Fe-hydride intermediate was postulated to form upon reduction of the Fe complex in the presence of phenol; conversely, an Fe-CO_2 intermediate was identified by a feature at 1804 cm^{-1} in the SEC-IR, and was observed to convert into an iron-carbonyl species (1847−1941 cm^{-1}). These, however, release CO very slowly, and therefore undergo competitive catalyst degradation.

Formic acid is the main product observed also in the case of Fe(N5), a reaction which, however, does not involve the formation of an iron hydride. In this case, the reactivity occurs at the Fe(I) state upon reaction with CO_2, forming an Fe(III)-CO_2^{2-} adduct; the authors ascribed the favored selectivity for formate to fast isomerization of the CO_2 ligand into the formate-type adduct, with respect to a slow C−O bond cleavage that would lead to the formation of CO.[38] Carbon monoxide was instead observed as the main product in the case of the analogous Co complex, under both electrochemical and photochemical conditions. Interestingly, this is one of few cases in which iron and cobalt centers bearing the same organic ligand both display CO_2 reduction catalysis. This Fe/Co similarity was observed also in the case of porphyrin derivatives, and of salophen and qpy complexes discussed below.

Fe(salophen) and Fe(qpy) are both active for catalytic CO production in the presence of phenol as the proton donor with a high initial selectivity (>99%), and involving Fe(I) intermediates.[39] In particular, Fe(salophen) evolves CO at $E = -2.0$ V vs Fc^+/Fc (FY up to 58%), while Fe(qpy) operates at a less negative potential of $E = -1.58$ V vs Fc^+/Fc (FY up to 48%). Both systems are, however, characterized by a limited TON of ca. 3 in the case of Fe(salophen), while TON = 8 for Fe(qpy). This limitation is again ascribable to competitive degradation pathways that lead to electrodeposition of iron nanoparticles at the working electrode. In the case of Fe(qpy), the critical step is a further reduction of an Fe(I)CO intermediate, active in the catalytic cycle, to a non-productive Fe(0)CO (identified by a peak at 1854 cm^{-1} in SEC-IR), with this latter being the one that undergoes demetalation and thus inducing electrodeposition of metallic iron. Interestingly, the durability of the Fe(qpy) catalyst is enhanced in photocatalytic cycles for reduction of CO_2, where the rate of the deleterious Fe(I)CO → Fe(0)CO reduction is lowered since it is controlled by diffusion processes; Fe(qpy) thus reaches TON = 1880 with 97% catalytic selectivity with $Ru(bpy)_3^{2+}$ as sensitizer and triethanolamine as sacrificial electron donor.

https://dx.doi.org/10.1021/acsomega.0c02786
ACS Omega 2020, 5, 21309−21319

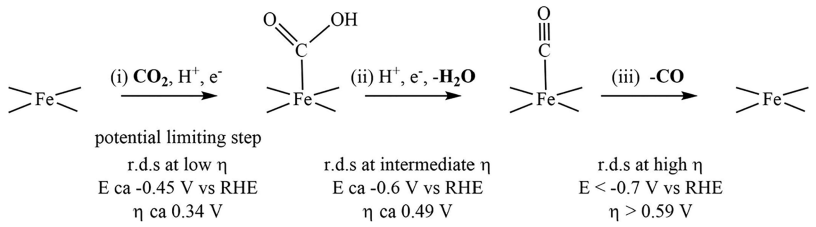

Figure 7. Mechanism of CO_2 reduction to CO with Fe single-atom sites.[43,44]

It is worth highlighting that in all the cases reported in this section, with the exception of Fe(N5), an iron carbonyl complex (Fe-CO) is detected as an intermediate, generated upon C−O bond cleavage at the Fe-CO_2 adduct (the C−O bond cleavage may be proton-assisted or, since instrumental features of the SEC-IR cell may limit the use of proton donors, can involve a second molecule of CO_2).[23] Iron carbonyl complexes have a vastly known and exploited chemistry, and the study of such intermediates by vibrational spectroscopy can indeed provide insights into the electronic environment of the catalytic active site. However, for the systems presented above, the experimentally observed Fe-CO adducts may represent turnover-limiting species, as observed for Fe(dophen) and Fe(^{tbu}dhbpy), or can be even responsible for catalyst decomposition (in the case of Fe(qpy), where the species observed by SEC-IR is an inert zerovalent iron carbonyl).

As a general principle in catalysis, observation of reaction intermediates should be met with caution. Their accumulation and spectroscopic characterization may in fact indicate a significant stability and inertness, suggesting that they could be possibly "out-of-the-cycle" intermediates. Furthermore, the iron carbonyl intermediates are a recurring motif in CO_2 reduction catalysts, showing an intrinsic degree of preference of such systems for reaction pathways that eventually lead to C−O bond cleavage.

IRON SINGLE-ATOM HETEROGENEOUS CATALYSTS

The large-scale utilization of a CO_2 reduction process requires the design of a device in which the catalysts can be ideally embedded in a low-cost, conductive material. Recently, several research groups have made efforts toward the design and preparation of iron single-atom catalysts, supported on nitrogen-doped carbon materials (Fe-N-C). This class of catalysts shows impressive analogies in terms of mechanism with coordination complexes discussed above.

Fe-N-C are prepared by pyrolysis of an iron precursor, together with a carbon source (typically a Zn-based zeolitic imidazolate framework, ZIF-8) and a nitrogen-containing organic ligand.[41,42] In these Fe-N-C materials, the active sites are identified as FeN_4 units,[41] resembling the coordination motif of molecular porphyrins, and being indeed selective toward the electrochemical reduction of CO_2 to CO in an aqueous environment (typically in bicarbonate electrolyte), while aggregated iron clusters or Fe-based nanoparticles favor the route toward hydrogen evolution.[41] The activity of FeN_4 sites was investigated theoretically, and a general operating mechanism involves (i) coordination of CO_2 to iron together with the addition of one electron and one proton to form an Fe-COOH site, (ii) addition of a second electron and a second proton, associated with the release of a water molecule and formation of an Fe-CO intermediate, and finally (iii) desorption of CO from the Fe site (Figure 7).[43−45] The activity for CO evolution is then determined by the Faradaic steps and by the adsorption energies of COOH and CO onto the Fe site.

In particular, the formation of the Fe-COOH adduct is predicted by simulations to be both the potential-limiting step and the rate-limiting step when a low overpotential is applied.[44] At intermediate overpotential, the rate-determining step involves the dissociative formation of H_2O with the production of the Fe-CO intermediate (Figure 7); consistently, the TOF is correlated to the CO binding energy descriptor (i.e., the higher the driving force of this step, the higher the rate). At higher overpotentials, the rate-limiting step is CO desorption, and in this region the hydrogen evolution reaction becomes competitive.[44] Interestingly, a strong binding of CO to the Fe site supports the partial formation of methane with this class of catalysts, since the bound CO can undergo the subsequent chemical steps necessary to arrive at CH_4 (see also previous discussion dealing with formation of methane with iron porphyrins).[46]

Recently, a couple of examples were reported dealing with a rational optimization of Fe single sites for enhancing the selectivity for CO production, while lowering the overpotential.[42,47] Zhang et al. selected a hemin ferric chloride as the iron source, thus providing a heme-like Fe(III) site bonded to the tetrapyrrole macrocycle, in combination with melamine as the nitrogen source. This resulted in the formation of FeN_5 sites, with an additional pyrrolic nitrogen coordinated at the apical position of iron; this reduces the Fe-to-CO π back-donation in the Fe-CO intermediate, thus favoring CO rapid desorption and boosting the selectivity, as predicted by DFT simulations.[47]

An even higher reactivity, with overpotential as low as 80 mV (in 0.5 M $KHCO_3$, saturated with CO_2), was observed for single-atom Fe(III)X_4 sites, with X = C and N (average coordination numbers are 3.4 and 0.5 for N and C, respectively).[42] In particular, the +3 oxidation state of iron was maintained along the catalysis, as revealed by operando X-ray absorption (XAS) spectroscopy; this feature was discussed to be crucial for the high reactivity, since Fe(III) guarantees faster CO_2 adsorption and CO desorption with respect to conventional Fe(II) sites. Also in this case the rate-determining step was postulated to be the protonation of the adsorbed CO_2^- to form the Fe-COOH intermediate at low overpotential. Conversely, CO desorption becomes rate determining at higher overpotential, parallel to the formation of Fe(II) sites; in these conditions, the material loses stability, due to a decrease in coordination number of Fe from 4 to 3.[42]

CONCLUSIONS AND PERSPECTIVES

The reduction of CO_2 has an intrinsic selectivity issue with respect to other reactions related to solar-to-fuel conversion

https://dx.doi.org/10.1021/acsomega.0c02786
ACS Omega 2020, 5, 21309−21319

(i.e., proton reduction to hydrogen or water oxidation to oxygen). Combining high reaction rates (i.e., current densities above 10^2 mA cm^{-2} in the case of electrolyzers) with high selectivity for a single product remains a challenge. The heterogeneous single-atom catalysts seem indeed very promising toward this application, considering also their easier scalability; the $Fe(III)X_4$ catalyst developed by Hu et al. operates with a current density of 94 mA cm^{-2} at 0.34 V overpotential, with >90% Faradaic yield for CO.[42] On the other hand, although their synthetic and functionalization procedures are often challenging, molecularly defined catalysts can offer advantages over heterogeneous materials, and can help in their design.[47]

The potential of molecular catalysts has been demonstrated by embedding cobalt phthalocyanine in a flow cell operating at >95% selectivity for CO at a current density of 150 mA cm^{-2};[48] this approach was recently extended to an iron porphyrin catalyst.[49] The role of molecular catalysts will be even more important in transformations where the selectivity target is more difficult to achieve, as in the case of highly reduced products of CO_2.

The control and orientation of selectivity are strictly connected to the comprehension of well-defined reaction mechanisms, as we have discussed in this Mini-Review for selected cases of iron coordination complexes. Formal electrokinetic analysis may be used to dissect the role of through-structure and through-space effects on each step of a catalytic mechanism. On the other hand, a complementary inorganic chemical approach based on experimental and computational techniques can be specifically devoted to clarifying the relationships binding together electronic and steric properties of the complexes, reactivity, and preferred reaction pathways. In this regard, theoretical calculations can be effectively integrated in the study of the catalytic mechanisms herein discussed. They provide fundamental quantitative and qualitative support to the interpretation of spectroscopic and electrochemical data, thus allowing a correct identification of the species involved and the determination of energetic profiles of possible reaction pathways. Furthermore, they can aid the study of catalytic systems involving second-sphere interactions, in which finely tuned catalyst−substrate adducts play a key role in justifying the superiority of such systems over simpler analogues.

These mutually integrating strategies make it possible not only to establish the role of key intermediates but also to steer their reactivity and enhance the selectivity of the overall process toward the desired reaction, while avoiding detrimental, turnover-limiting side reactions.

The ever-increasing corpus of design principles and investigation tools represents the key for a true, deep, rational implementation of the catalytic principles. This will eventually lead to the most effective, selective, and completely sustainable CO_2 reduction processes with the benefit of mechanistic knowledge and applications yet unreached.

AUTHOR INFORMATION

Corresponding Author

Andrea Sartorel − *Department of Chemical Sciences, University of Padova, 35131 Padova, Italy;* orcid.org/0000-0002-4310-3507; Email: andrea.sartorel@unipd.it

Authors

Ruggero Bonetto − *Department of Chemical Sciences, University of Padova, 35131 Padova, Italy;* orcid.org/0000-0002-6680-7910

Francesco Crisanti − *Department of Chemical Sciences, University of Padova, 35131 Padova, Italy;* orcid.org/0000-0002-7729-3767

Complete contact information is available at: https://pubs.acs.org/10.1021/acsomega.0c02786

Notes

The authors declare no competing financial interest.

Biographies

Ruggero Bonetto received his master's degree in chemistry cum laude in 2019 at the University of Padova. Currently, he is a Ph.D. student in molecular sciences at the same university, under the supervision of A.S. His research interests are inorganic and coordination chemistry, and he has developed a passion for electrochemistry related to catalytic reactions.

Francesco Crisanti received his bachelor's degree in chemistry in 2018 from the University of Padova, where he is now studying for his master's degree. His thesis project deals with the development of iron species for CO_2 reduction.

https://dx.doi.org/10.1021/acsomega.0c02786
ACS Omega 2020, 5, 21309−21319

Andrea Sartorel is an associate professor at the University of Padova and member of the Nano and Molecular Catalysis (NanoMolCat) Lab, based in the Department of Chemical Sciences. His research interests deal with electro- and photocatalysis for small molecule activation.

■ ACKNOWLEDGMENTS

A.S. acknowledges Fondazione Cariparo (project "Synergy", within the call Progetti di Eccellenza 2018) and the Department of Chemical Sciences at the University of Padova (Project PHOETRY, P-DiSC #10BIRD2018-UNIPD) for funding.

■ ABBREVIATIONS

CODHases = carbon monoxide dehydrogenases; FY = Faradaic yield; SEC-IR = spectroelectrochemistry in the infrared region; TON = turnover number; TOF = turnover frequency; NHE = normal hydrogen electrode; Fc^+/Fc = ferrocenium/ferrocene

■ REFERENCES

(1) Liu, Q.; Wu, L.; Jackstell, R.; Beller, M. Using Carbon Dioxide as a Building Block in Organic Synthesis. *Nat. Commun.* **2015**, *6*, 1−15.
(2) Francke, R.; Schille, B.; Roemelt, M. Homogeneously Catalyzed Electroreduction of Carbon Dioxide - Methods, Mechanisms, and Catalysts. *Chem. Rev.* **2018**, *118* (9), 4631−4701.
(3) Elouarzaki, K.; Kannan, V.; Jose, V.; Sabharwal, H. S.; Lee, J. M. Recent Trends, Benchmarking, and Challenges of Electrochemical Reduction of CO_2 by Molecular Catalysts. *Adv. Energy Mater.* **2019**, *9* (24), 1900090.
(4) Jeoung, J.-H.; Dobbek, H. Carbon Dioxide Activation at the Ni,Fe-Cluster of Anaerobic Carbon Monoxide Dehydrogenase. *Science* **2007**, *318* (5855), 1461−1464.
(5) Dobbek, H. Mechanism of Ni,Fe-Containing Carbon Monoxide Dehydrogenases. *Struct. Bonding (Berlin, Ger.)* **2018**, *179*, 153−166.
(6) Shin, W.; Lee, S. H.; Shin, J. W.; Lee, S. P.; Kim, Y. Highly Selective Electrocatalytic Conversion of CO_2 to CO at −0.57 V (NHE) by Carbon Monoxide Dehydrogenase from Moorella Thermoacetica. *J. Am. Chem. Soc.* **2003**, *125* (48), 14688−14689.
(7) Svetlitchnyi, V.; Peschel, C.; Acker, G.; Meyer, O. Two Membrane-Associated NiFeS-Carbon Monoxide Dehydrogenases from the Anaerobic Carbon-Monoxide-Utilizing Eubacterium Carboxydothermus Hydrogenoformans. *J. Bacteriol.* **2001**, *183* (17), 5134−5144.
(8) Ensign, S. A. Reactivity of Carbon Monoxide Dehydrogenase from Rhodospirillum Rubrum with Carbon Dioxide, Carbonyl Sulfide, and Carbon Disulfide. *Biochemistry* **1995**, *34* (16), 5372−5381.
(9) Waldie, K. M.; Ostericher, A. L.; Reineke, M. H.; Sasayama, A. F.; Kubiak, C. P. Hydricity of Transition-Metal Hydrides: Thermodynamic Considerations for CO_2 Reduction. *ACS Catal.* **2018**, *8* (2), 1313−1324.
(10) Rail, M. D.; Berben, L. A. Directing the Reactivity of $[HFe_4N(CO)_{12}]^-$ toward H^+ or CO_2 Reduction by Understanding the Electrocatalytic Mechanism. *J. Am. Chem. Soc.* **2011**, *133* (46), 18577−18579.
(11) Loewen, N. D.; Neelakantan, T. V.; Berben, L. A. Renewable Formate from C-H Bond Formation with CO_2: Using Iron Carbonyl Clusters as Electrocatalysts. *Acc. Chem. Res.* **2017**, *50* (9), 2362−2370.
(12) Taheri, A.; Thompson, E. J.; Fettinger, J. C.; Berben, L. A. An Iron Electrocatalyst for Selective Reduction of CO_2 to Formate in Water: Including Thermochemical Insights. *ACS Catal.* **2015**, *5* (12), 7140−7151.
(13) Taheri, A.; Carr, C. R.; Berben, L. A. Electrochemical Methods for Assessing Kinetic Factors in the Reduction of CO_2 to Formate: Implications for Improving Electrocatalyst Design. *ACS Catal.* **2018**, *8* (7), 5787−5793.
(14) Bi, J.; Hou, P.; Liu, F.; Kang, P. Electrocatalytic Reduction of CO_2 to Methanol by Iron Tetradentate Phosphine Complex Through Amidation Strategy. *ChemSusChem* **2019**, *12*, 2195−2201.
(15) Bonin, J.; Maurin, A.; Robert, M. Molecular Catalysis of the Electrochemical and Photochemical Reduction of CO_2 with Fe and Co Metal Based Complexes. Recent Advances. *Coord. Chem. Rev.* **2017**, *334*, 184−198.
(16) Costentin, C.; Robert, M.; Savéant, J.-M. Molecular Catalysis of Electrochemical Reactions. *Curr. Opin. Electrochem.* **2017**, *2* (1), 26−31.
(17) Costentin, C.; Robert, M.; Savéant, J. M. Current Issues in Molecular Catalysis Illustrated by Iron Porphyrins as Catalysts of the CO_2-to-CO Electrochemical Conversion. *Acc. Chem. Res.* **2015**, *48* (12), 2996−3006.
(18) Margarit, C. G.; Asimow, N. G.; Costentin, C.; Nocera, D. G. Tertiary Amine-Assisted Electroreduction of Carbon Dioxide to Formate Catalyzed by Iron Tetraphenylporphyrin. *ACS Energy Lett.* **2020**, *5* (1), 72−78.
(19) Römelt, C.; Song, J.; Tarrago, M.; Rees, J. A.; Van Gastel, M.; Weyhermüller, T.; Debeer, S.; Bill, E.; Neese, F.; Ye, S. Electronic Structure of a Formal Iron(0) Porphyrin Complex Relevant to CO_2 Reduction. *Inorg. Chem.* **2017**, *56* (8), 4745−4750.
(20) Römelt, C.; Ye, S.; Bill, E.; Weyhermüller, T.; Van Gastel, M.; Neese, F. Electronic Structure and Spin Multiplicity of Iron Tetraphenylporphyrins in Their Reduced States as Determined by a Combination of Resonance Raman Spectroscopy and Quantum Chemistry. *Inorg. Chem.* **2018**, *57* (4), 2141−2148.
(21) Davethu, P. A.; De Visser, S. P. CO_2 Reduction on an Iron-Porphyrin Center: A Computational Study. *J. Phys. Chem. A* **2019**, *123* (30), 6527−6535.
(22) Mondal, B.; Rana, A.; Sen, P.; Dey, A. Intermediates Involved in the $2e^-/2H^+$ Reduction of CO_2 to CO by Iron(0) Porphyrin. *J. Am. Chem. Soc.* **2015**, *137* (35), 11214−11217.
(23) Hammouche, M.; Lexa, D.; Savêant, J. M.; Momenteau, M. Chemical Catalysis of Electrochemical Reactions. Homogeneous Catalysis of the Electrochemical Reduction of Carbon Dioxide by Iron("0") Porphyrins. Role of the Addition of Magnesium Cations. *J. Am. Chem. Soc.* **1991**, *113* (22), 8455−8466.
(24) Costentin, C.; Robert, M.; Savéant, J.-M. Catalysis of the Electrochemical Reduction of Carbon Dioxide. *Chem. Soc. Rev.* **2013**, *42* (6), 2423−2436.
(25) Sen, P.; Mondal, B.; Saha, D.; Rana, A.; Dey, A. Role of 2nd Sphere H-Bonding Residues in Tuning the Kinetics of CO_2 Reduction to CO by Iron Porphyrin Complexes. *Dalt. Trans.* **2019**, *48* (18), 5965−5977.
(26) Bonin, J.; Chaussemier, M.; Robert, M.; Routier, M. Homogeneous Photocatalytic Reduction of CO_2 to CO Using Iron(0) Porphyrin Catalysts: Mechanism and Intrinsic Limitations. *ChemCatChem* **2014**, *6* (11), 3200−3207.
(27) Yoshikawa, S.; Choc, M. G.; O'Toole, M. C.; Caughey, W. S. An Infrared Study of CO Binding to Heart Cytochrome c Oxidase and Hemoglobin A. *J. Biol. Chem.* **1977**, *252* (15), 5498−5508.
(28) Costentin, C.; Drouet, S.; Robert, M.; Savéant, J. M. A Local Proton Source Enhances CO_2 Electroreduction to CO by a Molecular

https://dx.doi.org/10.1021/acsomega.0c02786
ACS Omega 2020, 5, 21309−21319

Fe Catalyst. *Science (Washington, DC, U. S.)* **2012**, *338* (6103), 90−94.
(29) Azcarate, I.; Costentin, C.; Robert, M.; Savéant, J. M. Through-Space Charge Interaction Substituent Effects in Molecular Catalysis Leading to the Design of the Most Efficient Catalyst of CO_2-to-CO Electrochemical Conversion. *J. Am. Chem. Soc.* **2016**, *138* (51), 16639−16644.
(30) Gotico, P.; Boitrel, B.; Guillot, R.; Sircoglou, M.; Quaranta, A.; Halime, Z.; Leibl, W.; Aukauloo, A. Second-Sphere Biomimetic Multipoint Hydrogen-Bonding Patterns to Boost CO_2 Reduction of Iron Porphyrins. *Angew. Chem., Int. Ed.* **2019**, *58* (14), 4504−4509.
(31) Nichols, A. W.; Machan, C. W. Secondary-Sphere Effects in Molecular Electrocatalytic CO_2 Reduction. *Front. Chem.* **2019**, *7*, 1−19.
(32) Bonin, J.; Robert, M.; Routier, M. Selective and Efficient Photocatalytic CO_2 Reduction to CO Using Visible Light and an Iron-Based Homogeneous Catalyst. *J. Am. Chem. Soc.* **2014**, *136* (48), 16768−16771.
(33) Genoni, A.; Chirdon, D. N.; Boniolo, M.; Sartorel, A.; Bernhard, S.; Bonchio, M. Tuning Iridium Photocatalysts and Light Irradiation for Enhanced CO_2 Reduction. *ACS Catal.* **2017**, *7* (1), 154−160.
(34) Rao, H.; Bonin, J.; Robert, M. Visible-Light Homogeneous Photocatalytic Conversion of CO_2 into CO in Aqueous Solutions with an Iron Catalyst. *ChemSusChem* **2017**, *10*, 4447−4450.
(35) Rao, H.; Lim, C. H.; Bonin, J.; Miyake, G. M.; Robert, M. Visible-Light-Driven Conversion of CO_2 to CH_4 with an Organic Sensitizer and an Iron Porphyrin Catalyst. *J. Am. Chem. Soc.* **2018**, *140* (51), 17830−17834.
(36) Pun, S. N.; Chung, W. H.; Lam, K. M.; Guo, P.; Chan, P. H.; Wong, K. Y.; Che, C. M.; Chen, T. Y.; Peng, S. M. Iron(I) Complexes of 2,9-Bis(2-Hydroxyphenyl)-1,10-Phenanthroline (H_2dophen) as Electrocatalysts for Carbon Dioxide Reduction. X-Ray Crystal Structures of $[Fe(Dophen)Cl]_2{\cdot}2HCON(CH_3)_2$ and $[Fe(Dophen)(N\text{-}MeIm)_2]ClO_4$ (N-MeIm = 1-Methylimidazole). *J. Chem. Soc. Dalt. Trans.* **2002**, No. 4, 575−583.
(37) Nichols, A. W.; Chatterjee, S.; Sabat, M.; MacHan, C. W. Electrocatalytic Reduction of CO_2 to Formate by an Iron Schiff Base Complex. *Inorg. Chem.* **2018**, *57* (4), 2111−2121.
(38) Chen, L.; Guo, Z.; Wei, X. G.; Gallenkamp, C.; Bonin, J.; Anxolabéhère-Mallart, E.; Lau, K. C.; Lau, T. C.; Robert, M. Molecular Catalysis of the Electrochemical and Photochemical Reduction of CO_2 with Earth-Abundant Metal Complexes. Selective Production of CO vs HCOOH by Switching of the Metal Center. *J. Am. Chem. Soc.* **2015**, *137* (34), 10918−10921.
(39) Cometto, C.; Chen, L.; Lo, P. K.; Guo, Z.; Lau, K. C.; Anxolabéhère-Mallart, E.; Fave, C.; Lau, T. C.; Robert, M. Highly Selective Molecular Catalysts for the CO_2-to-CO Electrochemical Conversion at Very Low Overpotential. Contrasting Fe vs Co Quaterpyridine Complexes upon Mechanistic Studies. *ACS Catal.* **2018**, *8* (4), 3411−3417.
(40) Bonetto, R.; Altieri, R.; Tagliapietra, M.; Barbon, A.; Bonchio, M.; Robert, M.; Sartorel, A. Electrochemical Conversion of CO_2 to CO by a Competent Fe(I) Intermediate Bearing a Schiff Base Ligand. *ChemSusChem* **2020**, DOI: 10.1002/cssc.202001143.
(41) Huan, T. N.; Ranjbar, N.; Rousse, G.; Sougrati, M.; Zitolo, A.; Mougel, V.; Jaouen, F.; Fontecave, M. Electrochemical Reduction of CO_2 Catalyzed by Fe-N-C Materials: A Structure-Selectivity Study. *ACS Catal.* **2017**, *7* (3), 1520−1525.
(42) Gu, J.; Hsu, C. S.; Bai, L.; Chen, H. M.; Hu, X. Atomically Dispersed Fe^{3+} Sites Catalyze Efficient CO_2 Electroreduction to CO. *Science (Washington, DC, U. S.)* **2019**, *364* (6445), 1091−1094.
(43) Hansen, H. A.; Varley, J. B.; Peterson, A. A.; Nørskov, J. K. Understanding Trends in the Electrocatalytic Activity of Metals and Enzymes for CO_2 Reduction to CO. *J. Phys. Chem. Lett.* **2013**, *4* (3), 388−392.
(44) Ju, W.; Bagger, A.; Hao, G. P.; Varela, A. S.; Sinev, I.; Bon, V.; Roldan Cuenya, B.; Kaskel, S.; Rossmeisl, J.; Strasser, P. Understanding Activity and Selectivity of Metal-Nitrogen-Doped Carbon Catalysts for Electrochemical Reduction of CO_2. *Nat. Commun.* **2017**, *8* (1), 1−9.
(45) Pan, F.; Zhang, H.; Liu, K.; Cullen, D.; More, K.; Wang, M.; Feng, Z.; Wang, G.; Wu, G.; Li, Y. Unveiling Active Sites of CO_2 Reduction on Nitrogen-Coordinated and Atomically Dispersed Iron and Cobalt Catalysts. *ACS Catal.* **2018**, *8* (4), 3116−3122.
(46) Back, S.; Lim, J.; Kim, N. Y.; Kim, Y. H.; Jung, Y. Single-Atom Catalysts for CO_2 Electroreduction with Significant Activity and Selectivity Improvements. *Chem. Sci.* **2017**, *8* (2), 1090−1096.
(47) Zhang, H.; Li, J.; Xi, S.; Du, Y.; Hai, X.; Wang, J.; Xu, H.; Wu, G.; Zhang, J.; Lu, J.; Wang, J. A Graphene-Supported Single-Atom FeN5 Catalytic Site for Efficient Electrochemical CO_2 Reduction. *Angew. Chem., Int. Ed.* **2019**, *58* (42), 14871−14876.
(48) Ren, S.; Joulié, D.; Salvatore, D.; Torbensen, K.; Wang, M.; Robert, M.; Berlinguette, C. P. Molecular Electrocatalysts Can Mediate Fast, Selective CO_2 Reduction in a Flow Cell. *Science (Washington, DC, U. S.)* **2019**, *365* (6451), 367−369.
(49) Torbensen, K.; Han, C.; Boudy, B.; von Wolff, N.; Bertail, C.; Braun, W.; Robert, M. Iron Porphyrin Allows Fast and Selective Electrocatalytic Conversion of CO_2 to CO in a Flow Cell. *Chem. - Eur. J.* **2020**, *26* (14), 3034−3038.

https://dx.doi.org/10.1021/acsomega.0c02786
ACS Omega 2020, 5, 21309−21319